Nuclear quantum effect and temperature dependency on the hydrogen-bonded structure of 7-azaindole dimer

ARTICLE *in* THEORETICAL CHEMISTRY ACCOUNTS · SEPTEMBER 2014

Impact Factor: 2.23 · DOI: 10.1007/s00214-014-1553-y

4 AUTHORS, INCLUDING:

Nawee Kungwan
Chiang Mai University
55 PUBLICATIONS **217** CITATIONS
SEE PROFILE

Supa Hannongbua
Kasetsart University
175 PUBLICATIONS **1,381** CITATIONS
SEE PROFILE

Theor Chem Acc (2014) 133:1553
DOI 10.1007/s00214-014-1553-y

REGULAR ARTICLE

Nuclear quantum effect and temperature dependency on the hydrogen-bonded structure of 7-azaindole dimer

Nawee Kungwan · Yudai Ogata · Supa Hannongbua · Masanori Tachikawa

Received: 2 April 2014 / Accepted: 26 July 2014

Abstract The structure of 7-azaindole dimer ($7AI_2$) as a model compound for DNA base pair has been studied by classical molecular dynamics (MD) and path integral molecular dynamics (PIMD) simulations on the semi-empirical PM6 potential energy surface at various temperatures, to investigate the nuclear quantum effect and temperature dependency on the hydrogen-bonded moiety of $7AI_2$. At 75 K, two H-bondings are maintained throughout a given simulation time in both classical and PIMD (quantum) simulations. At 150 K, these two H-bondings are maintained in only quantum simulation, while in classical simulation, the two H-bondings (or one H-bonding) are sometimes broken and reformed. For 225 K, these two H-bondings are broken in both classical and quantum simulations. We have also applied a principal component analysis to MD and PIMD simulations to analyze the intermolecular motions. We found that the ratio of the second lowest (dimer butterfly out-of-plane) vibrational mode from normal mode analysis which is the most dominant motion decreases with increasing temperature, whereas that of first lowest (dimer torsion out-of-plane) vibrational mode which is the second most dominant motion increases with increasing temperature from temperature 75 to 150 K and then decreases at 225 K due to the nuclear quantum effect. Moreover, the motions of two hydrogen-bonded structures are significantly different with increasing temperature. This difference is revealed by the principal component analysis which shows that the ratio of opening in-plane motion decreases and the ratio of stretching in-plane motion decreases.

Keywords 7-Azaindole dimer · Path integral simulation · Nuclear quantum effect

1 Introduction

Hydrogen-bonded amino compounds, abundant in nature, play a crucial role in the biological function of DNA and in the secondary protein structure [1]. In these amino compounds, a nitrogen atom donates hydrogen or proton to a proton acceptor atom such as oxygen or nitrogen. In the case of DNA, the N–H groups of the nucleobase pairs constitute the double-stranded structure enabling genetic coding. Moreover, the hydrogen bond strength determines the likelihood of hydrogen or proton transfer between the donating and accepting groups, leading to a tautomerization. For elucidation of the complicated function of nucleobase pairs in the DNA, model compounds with their doubly or triply hydrogen-bonded structure have been studied. The dimer of 7-azaindole ($7AI_2$) has been regarded as a model for the hydrogen-bonded DNA base pairs and has been suggested to provide information about the mechanism involving the mutation of DNA [2]. For this reason,

Electronic supplementary material The online version of this article (doi:10.1007/s00214-014-1553-y) contains supplementary material, which is available to authorized users.

N. Kungwan (✉)
Department of Chemistry, Faculty of Science, Chiang Mai University, Chiang Mai 50200, Thailand
e-mail: naweekung@gmail.com

Y. Ogata · M. Tachikawa (✉)
Quantum Chemistry Division, Graduate School of Nanobioscience, Yokohama City University, Yokohama 236-0027, Japan
e-mail: tachi@yokohama-cu.ac.jp

S. Hannongbua
Department of Chemistry, Faculty of Science, Kasetsart University, Bangkhen Campus, Bangkok 10930, Thailand

Published online: 09 August 2014

the excited state dynamics of $7AI_2$ has been intensively investigated using ultrafast spectroscopic techniques and theoretical studies [3–6]. The mechanism of proton transfer (either concerted or stepwise) has been extensively discussed among several groups [3, 5–9], but it is still in controversy. For the ground state dynamics of $7AI_2$, the investigation is not extensive [10–13]. However, such a dynamics study in the ground state is important in many chemical reactions, such as acid–base reaction.

Structure and intermolecular vibrations of hydrogen-bonded $7AI_2$ in normal form were studied by IR dip spectroscopy [14] and a supersonic jet expansion [15]. Hazra et al. [15] found 7AI dimer with one water to be the most abundant species at 353 K which is contrary to other findings of 7AI dimer in low temperatures [4, 16]. Vibrational frequency assignment of both techniques was helped with quantum chemical calculation. The combined theoretical and spectroscopic study has shown that the vibrational spectrum of $7AI_2$ was dramatically influenced by the two intermolecular hydrogen bonds [17]. Dimerization of 7AI also strongly affects its vibrational dynamics as it has been reported by femtosecond infrared pump–probe measurement comparing the N–H stretching dynamics of monomer and dimmers [17, 18]. Recently, a large deuteration effect on the NH/ND stretch band [19, 20] has been observed due to a large anharmonicity of the potential energy surface originating from the double hydrogen-bonded dimer.

Most theoretical calculations on $7AI_2$ have been carried out by a simple normal mode analysis. These calculations normally compute the approximation of nucleus as a classical point charge. However, the quantum effect of vibration in addition to anharmonic and mode coupling effects could play a role in better description of hydrogen-bonded systems. There have been some reports that the quantum effect is indispensable for understanding of some hydrogen-bonded system [21–23]. To the best of our knowledge, there is no report about the nuclear quantum effect and temperature dependency on $7AI_2$ structure. There are a few of recent reports on the nuclear quantum effect using an MD and PIMD simulation that was carried out for DNA model structure by Perez et al. [24], but they did not include purine and pyrimidine rings to investigate the stability of the tautomeric forms of base pairs. Recently, our group [25, 26] have studied nuclear quantum effect and temperature dependency on the hydrogen-bonded structure of A–T and G–C pairs at 300 K. Despite several theoretical reports on the potential enol tautomers of DNA base pairs, to date, there is no direct experimental evidence to support these theoretical findings. Therefore, it is important to study the DNA model structure, especially the model compound whose spectroscopic data have been intensively investigated like the $7AI_2$.

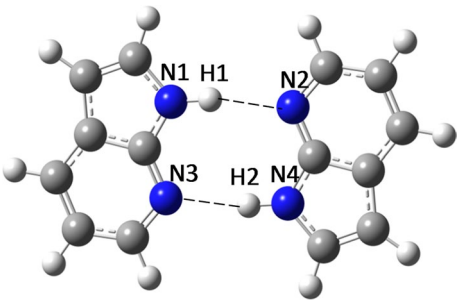

Fig. 1 Structure and atomic labeling of $7AI_2$ normal form

In this work, we report MD and PIMD simulations of DNA model compound, $7AI_2$ structure, in the gas phase (Fig. 1). The nuclear quantum effect influencing on the hydrogen-bonded structure of $7AI_2$ has been studied at several temperatures. The principal component analysis was also employed to study the nuclear quantum effect on intermolecular motions of $7AI_2$.

2 Computational details

Semiempirical PM6 method [27] was employed for all electronic structure calculations. The PM6 method has been used in our previous study and proved to be acceptable in the case of isolated G–C base pair [26]. The validation of this method is provided by comparison the structural information of optimized $7AI_2$ with various ab initio and density functional theory levels. The values at PM6 levels were calculated using MOPAC2009 program package [28], while the values at RI-BVWN, RI-MP2, and RI-CC2 levels were obtained using TURBOMOLE program package [29]. The other values at HF and B3LYP levels are computed with G03 program package [30].

The classical molecular dynamics (MD) and path integral molecular dynamics (PIMD) simulations have been used for $7AI_2$ with Nosé–Hoover chain thermostats [31] to achieve a canonical ensemble in the same way as in the previous work [32] (see also computational detail and path integral methodology in ref. [33–39]). In our PIMD simulation, we have used normal mode coordinates instead of the real space coordinates. This is because the directly applying the effective Hamiltonian for path integral method to canonical equation of motion is known to be inefficient. To solve this difficulty, we introduce the normal mode coordinates as the nuclear coordinates combined with massive Nosé–Hoover chain technique. To find out more details, please refer to references [38, 39]. The simulations were carried out at temperatures of 75, 150, and 225 K. The simulations at 300 K were also performed, but the dissociation to 7AI monomers was observed, so we analyzed our

data with conditions below 300 K. The PIMD simulation (or "quantum simulation") which takes both thermal and quantum fluctuations into account has been performed with number of beads $P = 64$ at 75 K, $P = 32$ at 150 K, and $P = 24$ at 225 K, as in previous studies [26, 32, 40]. The quantum simulations were performed for 90,000 steps with the step size $\Delta t = 0.1$ fs at all temperatures after a thermal equilibrium run of 1,000 steps. The MD simulations (or "classical simulation") were performed for 1,500,000 steps with $\Delta t = 0.1$ fs after equilibrium run of 1,000 steps. The convergence data of kinetic energies with primitive and virial energy estimators at 75 and 150 K are shown in Figure S1 of the Supporting Information.

3 Results and discussion

3.1 Preliminary static molecular orbital calculation

To validate the PM6 method, structural parameters of optimized $7AI_2$ normal form (important atoms are labeled as in Fig. 1) and the first six lowest vibrational frequencies were compared with other methods, along with reference as listed in Table 1. The full vibrational frequencies of optimized $7AI_2$ normal form are listed in Table S1 of the Supporting Information. From Table 1 and Table S1 of the Supporting Information, results from PM6 tend to underestimate the vibrational frequencies of $7AI_2$ normal form as compared to other methods (NH stretching is very good agreement with available experiment data). For the covalent-bonded NH distances (R_{N1H1} and R_{N3H2}), the values of PM6 at 1.021 Å are close to those of DFT (B3LYP and RI-BVWN), RI-CC2, and references [MP2/Sapporo-DZP and MP2/6-31G(d,p)] reported by Taketsugu et al. [41] and Hazra et al. [15], while they are slightly longer than the results of HF. The symmetry of $7AI_2$ normal form optimized at PM6 was found to be C_{2h} which is the same symmetry as in MP2, RI-MP2, and RI-CC2 results. The values of the hydrogen-bonded distances of PM6 are in between the values of HF and RI-CC2. Contrary to the covalent-bonded distances, the $R_{H1\cdots N2}$ and $R_{H2\cdots N3}$, and two heavy atomic distances ($R_{N1\cdots N2}$ and $R_{N3\cdots N4}$) of hydrogen bond are slightly longer than those from other methods. From Table 1, thus, PM6 is found to be qualitatively sufficient to describe the stable structure of the hydrogen bonds of $7AI_2$.

3.2 Nuclear quantum effect on the hydrogen-bonded structure

In this section, geometrical parameters affecting by the nuclear quantum effect in the hydrogen-bonded structure at different temperatures were analyzed. First, we focus on the overall behavior of the two H-bondings in hydrogen-bonded $7AI_2$ structure. Since the complete dissociation of $7AI_2$ structure was observed at high temperatures, results with simulation temperature below 300 K were given. At 75 K, two H-bondings are maintained throughout a given simulation time in both classical and quantum simulations. At 150 K, these two H-bondings are maintained in only quantum simulation, while in classical simulation, the two H-bondings (or one H-bonding) are sometimes broken and reformed (two 7AI molecules separate from each other but come close to each other to form H-bondings again). For 225 K, these two H-bondings are broken in both classical and quantum simulations.

Table 1 Structural parameters (Å) of two hydrogen bonds in 7AI dimer and vibrational frequencies (cm^{-1}) of first six lowest vibrational modes with PM6, HF/6-31+G(d,p), B3LYP/6-31+G(d,p), and RI-BVWN/SVP levels of calculations, along with references (MP2 and DF spectrum)

	Geometry						Vibrational mode					
	R_{N1H1}	R_{N4H2}	$R_{H1\cdots N2}$	$R_{H2\cdots N3}$	$R_{N1\cdots N2}$	$R_{N3\cdots N4}$	ω_1	ω_2	ω_3	ω_4	ω_5	ω_6
PM6	1.021	1.021	2.134	2.134	3.148	3.148	25	29	59	63	66	80
HF/6-31G(d,p)	1.003	1.003	2.117	2.114	3.114	3.111	22	33	66	82	85	94
B3LYP/6-31G(d,p)	1.031	1.033	1.915	1.917	2.942	2.943	26	34	81	91	100	111
RI-BVWN/SVP	1.040	1.040	1.969	1.969	3.002	3.003	29	36	75	94	94	102
RI-MP2/SVP	1.041	1.041	1.851	1.851	2.887	2.887						
RI-CC2/SVP	1.045	1.045	1.830	1.830	2.870	2.870						
Reference												
Expt.[a]												110
MP2/Sapporo-DZP	1.038	1.038	1.864	1.864	2.902	2.902						
MP2/6-31G(d,p)	1.031	1.031	1.893	1.893	2.919	2.919	23	34	81	86	94	115

ω_1 dimer torsion out-of-plane (oop), ω_2 dimer butterfly oop, ω_3 dimer opening in-plane (ip), ω_4 dimer stagger oop, ω_5 dimer sliding ip, and ω_6 dimer stretching ip

[a] DF spectrum from ref. [19]

3.2.1 *One-dimensional analysis*

For nuclear quantum effect on the hydrogen-bonded moiety of $7AI_2$ at several different temperatures, one-dimensional analyses on distributions of some important covalent and non-covalent bond distances at 75 and 150 K are shown in Fig. 2, and those at 225 K in Figure S2 of the Supporting Information, where the superscripts (Qm), (Cl), and (Eq) stand for quantum, classical, and equilibrium structures, respectively. For covalent NH bond lengths, average values and statistical errors at 75, 150, and 225 K on $7AI_2$, together with the Eq values, are listed in Table 2. Please note that the Eq values are obtained from static molecular orbital calculations.

From Fig. 2a, b, it can be seen that the R_{NH} distributions from classical simulations have sharp peaks around the equilibrium values, while those from quantum calculations are more broadened due to the mainly zero-point motion. From Table 2, covalent NH bond lengths with quantum simulations are found to be systematically longer than those with classical simulations and the Eq value, whereas the bond lengths with classical simulations

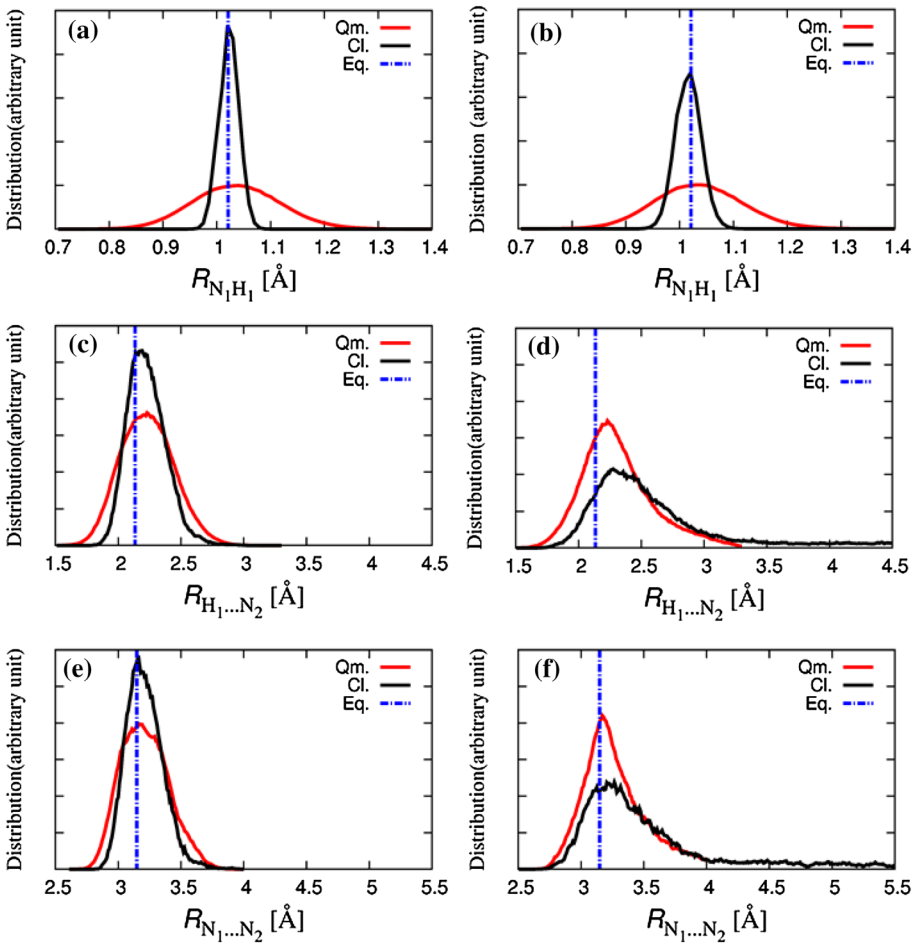

Fig. 2 One-dimensional distributions of important **a** R_{N1H1} at 75 K, **b** R_{N1H1} at 150 K, **c** $R_{H1\cdots N2}$ at 75 K, **d** $R_{H1\cdots N2}$ at 150 K, **e** $R_{N1\cdots N2}$ at 75 K, and **f** $R_{N1\cdots N2}$ at 150 K with quantum (Qm.) and classical (Cl.) simulations, as well as the equilibrium (Eq.) values, respectively

Table 2 Average values and statistical errors of the covalent bond lengths (R_{NH}) and the hydrogen-bonded distances between heavy atoms ($R_{N\cdots N}$) and hydrogen atom ($R_{H\cdots N}$) with quantum and classical simulations (at 75, 150, and 225 K), as well as the equilibrium values

	Quantum			Classical			Equilibrium
	75 K	150 K	225 K	75 K	150 K	225 K	
R_{N1H1}	1.035 (0.000)	1.03 3(0.000)	1.025 (0.005)	1.020 (0.000)	1.013 (0.002)	1.015 (0.001)	1.021
$R_{H1\cdots N2}$	2.228 (0.045)	2.311 (0.020)	3.759 (0.400)	2.222 (0.012)	3.378 (0.800)	3.482 (0.270)	2.134
$R_{N1\cdots N2}$	3.209 (0.020)	3.273 (0.045)	4.340 (1.000)	3.206 (0.015)	4.051 (0.750)	4.141 (0.300)	3.148

are close to the Eq values. These results are observed at all temperatures, showing that nuclear quantum effect has the significant contribution to the anharmonicity of the covalent NH bond at low temperature below 150 K, while at 225 K, this quantum effect has less significant contribution.

The distributions of hydrogen-bonded distances measured between hydrogen atom and heavy atom ($R_{H1\cdots N2}$ and $R_{N1\cdots N2}$) can be seen in Fig. 2c, d and Figure S1 of the Supporting Information and the values along with statistical errors are listed in Table 2. The peak positions of $R_{H1\cdots N2}$ in the quantum simulation are found to be close to the corresponding equilibrium values at 75 and 150 K, while they are longer at 225 K. For classical simulation, the average values at 75 K are found to be close to the corresponding equilibrium values, while they are longer at 150 and 225 K. In Fig. 2d at 150 K, the distribution of classical simulation is found to be broader than that of quantum simulation, contrary to the Fig. 2c at 75 K. We address here again that at 150 K the two H-bondings are maintained in only quantum simulation, while the two H-bondings (or one H-bonding) are sometimes broken and reformed in classical simulation.

For distances between two heavy atoms ($R_{N1\cdots N2}$), the one-dimensional distributions are shown in Fig. 2e, f and the average values along with the errors are listed in Table 2. Similar to the $R_{H1\cdots N2}$ distances, the peak positions of $R_{N1\cdots N2}$ in quantum simulation are close to the Eq values at 75 and 150 K, whereas they are longer at 225 K. For classical simulation results, these values are found to be close to the corresponding Eq values at 75 K, but they are relatively longer at 150 and 225 K. Again, the two H-bondings (or one H-bonding) are sometimes broken and reformed at 150 K in classical simulation. Thus, the quantum effect enhances the H-bonding around this temperature region.

3.2.2 *Two-dimensional analysis*

Two-dimensional correlations between the distances R_{NH} and $R_{N\cdots N}$, and between the distance $R_{H\cdots N}$ and $R_{N\cdots N}$, as has been done in the previous studies for various hydrogen-bonded systems [26, 36, 42–44], are plotted in Figs. 3 and 4, respectively (also in Figure S3 of the Supporting Information for temperature at 225 K). The shapes of two-dimensional distributions in Fig. 3 indicate the weak

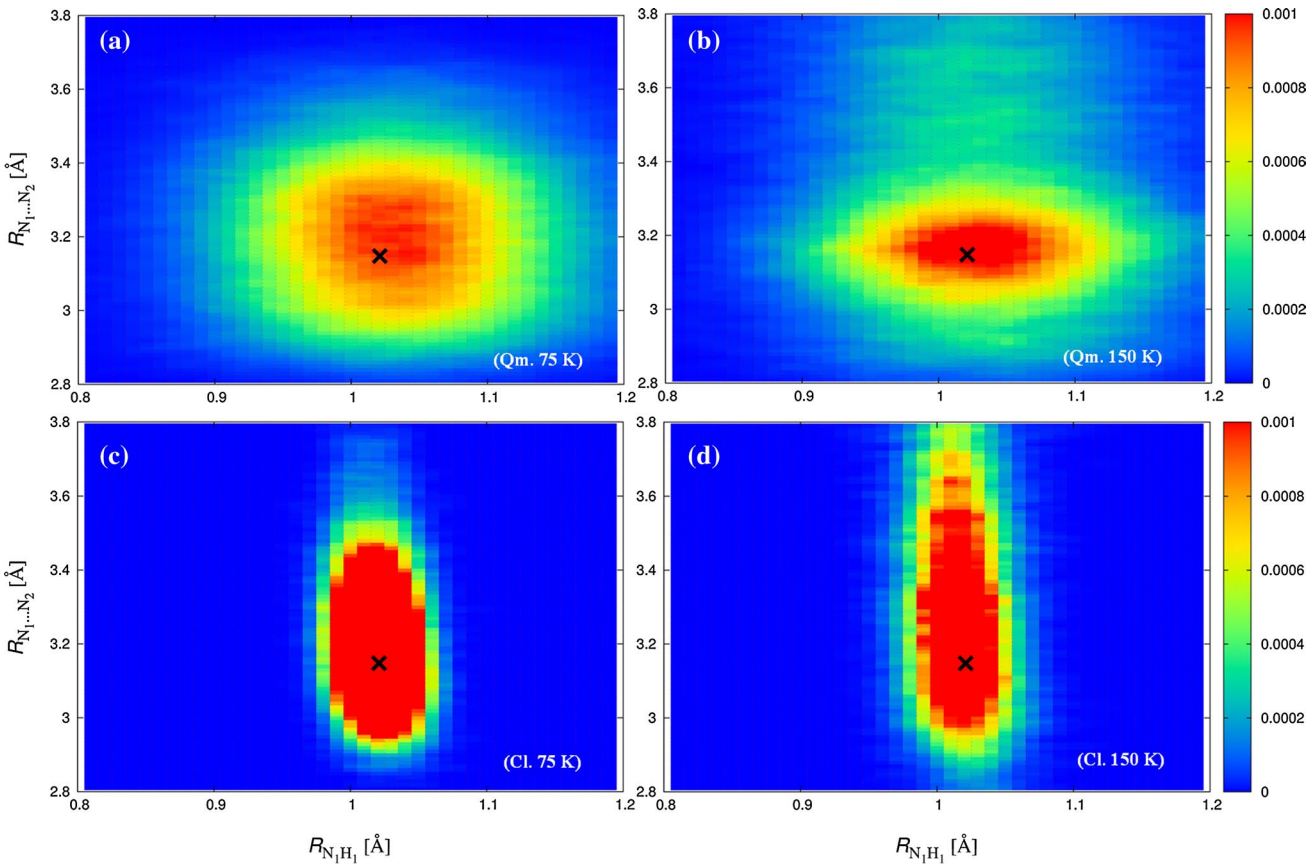

Fig. 3 Two-dimensional distributions of R_{N1H1} and $R_{N1\cdots N2}$ distances **a** quantum at 75 K, **b** quantum at 150 K, **c** classical at 75 K, and **d** classical at 150 K

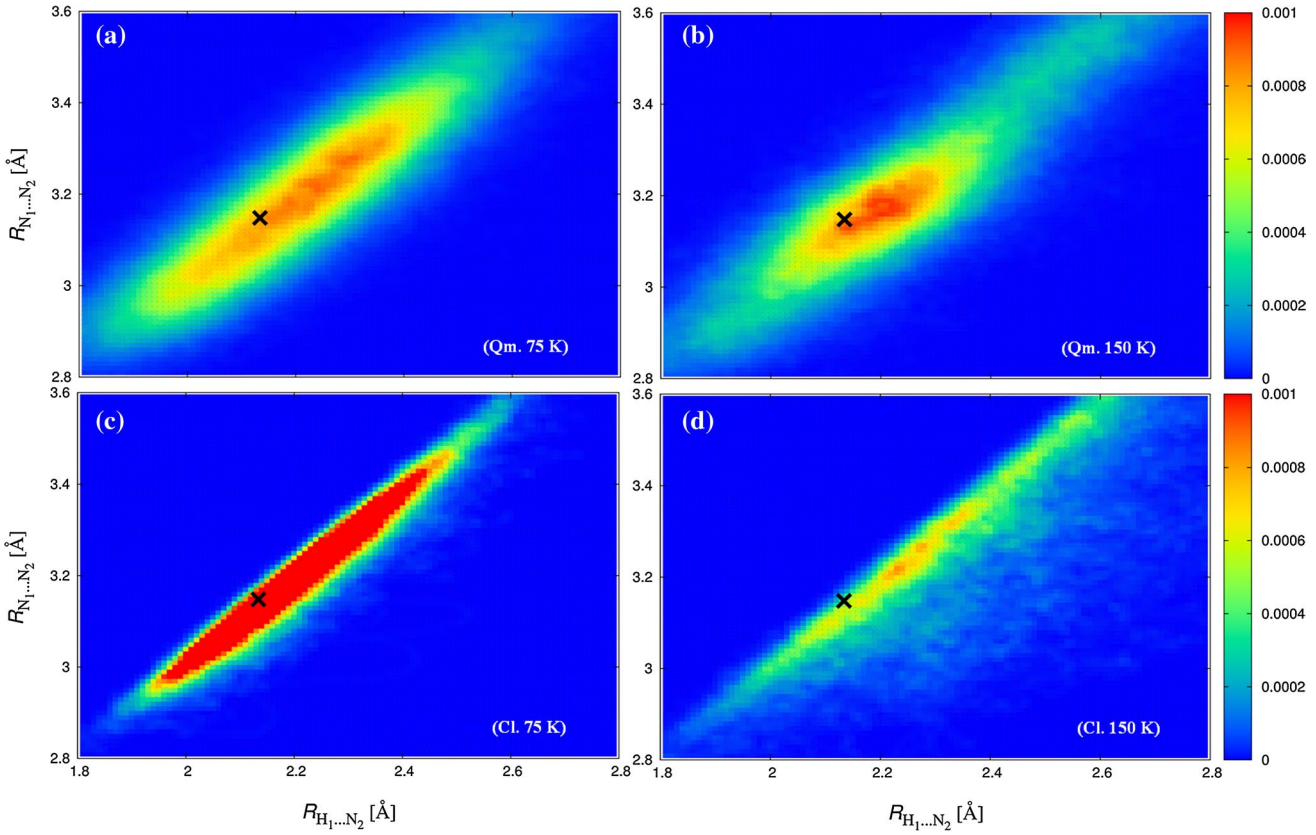

Fig. 4 Two-dimensional distributions of $R_{H1\cdots N2}$ and $R_{N1\cdots N2}$ distances **a** quantum at 75 K, **b** quantum at 150 K, **c** classical at 75 K, and **d** classical at 150 K

correlation between the NH and N···N distances at all temperatures for both quantum and classical simulations. While the N···N distance strongly correlates with the H···N distance as it can be seen in Fig. 4, this strong correlation becomes very weak at 225 K because hydrogen-bonded structure of $7AI_2$ starts to dissociate from each other.

Here, we would like to focus on the two-dimensional distributions with respect to $R_{N1\cdots N2}$ and $R_{N3\cdots N4}$ shown in Fig. 5. Figure 5a, b is the distributions obtained by quantum and classical simulations at 75 K, respectively. Similar to Fig. 5a–d are the distributions obtained by quantum and classical simulations at 150 K. We are able to see positive correlations between $R_{N1\cdots N2}$ and $R_{N3\cdots N4}$ in both quantum and classical simulations at 75 K from Fig. 5a, b. On the other hand, the cross-shaped distribution is seen in quantum simulation at 150 K from Fig. 5c. These differences indicate that $R_{N1\cdots N2}$ and $R_{N3\cdots N4}$ elongate simultaneously at 75 K, i.e., the stretching motion between 7AI monomers contributes largely to the whole molecular motions relative to the case at 150 K. To analyze the driving force of the cross-shaped distribution in Fig. 5c, we need to employ principal component analysis in the next section. We found the much weaker correlation in Fig. 5d. This is because that $7AI_2$ are dissociated due to thermal fluctuation. The much weaker correlation between $R_{N1\cdots N2}$ and $R_{N3\cdots N4}$ are also found at 225 K for both quantum and classical simulations, as shown in Figure S4 of the Supporting Information.

The dissociation of $7AI_2$ was observed in both quantum and classical simulations at 300 K, supporting the finding in ref [4, 16]. Our results suggest that in free-jet experiments [45, 46] with the sample reservoir being heating up to 393 K, the 7AI emerging from the nozzle could be the only monomeric species. If there is some water present in the sample reservoir, however, the complex of $7AI_2$ with water [14, 15] can be observed.

3.3 Nuclear quantum effect on intermolecular motions: principal component analysis

Principal component analysis (PCA), the same as the effective normal mode analysis [47], was employed to study the nuclear quantum effect on the molecular motion of $7AI_2$ from classical and quantum simulations. PCA is a widely used technique to retrieve dominant patterns on statistical data [48–51]. In this work, new variables of principal component (PC) representing the displacement of the whole

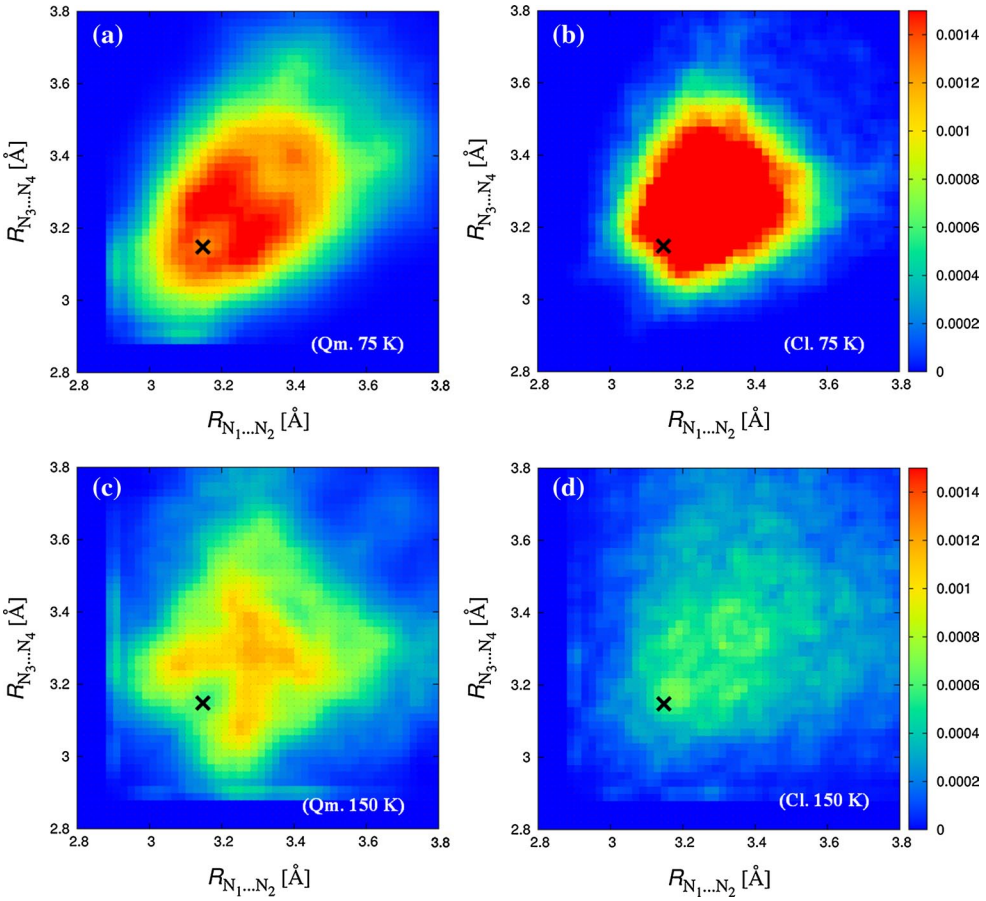

Fig. 5 Two-dimensional distributions of two heavy atomic distances ($R_{N1\cdots N2}$ and $R_{N3\cdots N4}$) **a** quantum at 75 K, **b** classical at 75 K, **c** quantum at 150 K, and **d** classical at 150 K

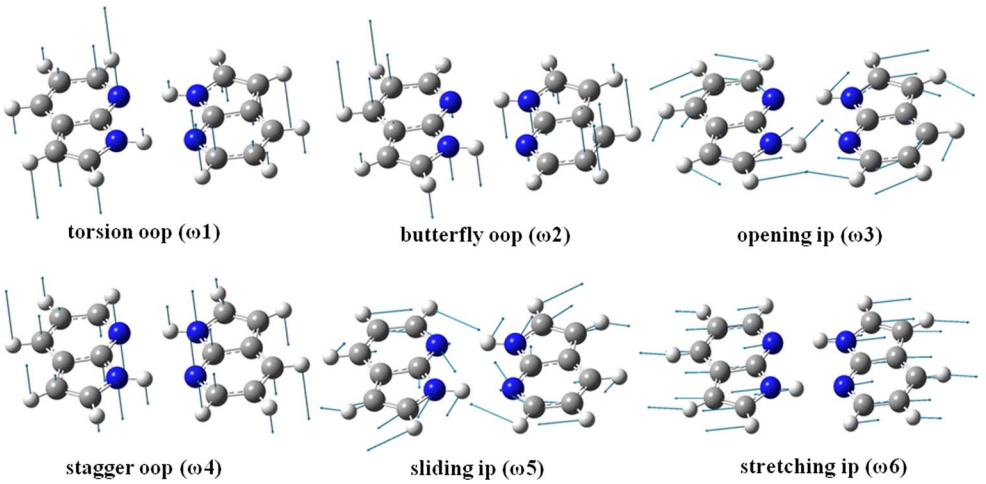

Fig. 6 Computed six lowest vibrational modes of 7AI dimer at PM6

molecule are computed from the displacement of each atom in trajectories of classical and quantum simulations. The motions of the largest six PCs for $7AI_2$ are torsion out-of-plane (oop) (ω_1), butterfly oop (ω_2), opening in-plane (ip) (ω_3), stagger oop (ω_4), sliding ip (ω_5), and stretching ip (ω_6) as illustrated in Fig. 6 and listed in Table 1. These PCs correspond to the six lowest vibrational normal modes as they were assigned in previous reports by Hazra et al. [15] and Dreyer [17]. The contributing ratios of all six modes to the fluctuation of the whole molecular motions are listed in Table 3.

From Table 3, butterfly and torsion oop modes of dimer are found to be dominant contributors in quantum and classical simulations about 38–78 % of the whole molecular motion. The contributing ratios of sliding ip and stretching ip are both about 10 %, while those of opening ip and

Table 3 Contribution ratios of ω_1–ω_6 (described in Table 1) in $7AI_2$ at respective temperatures from quantum and classical simulations

Vibrational mode	75 K		150 K		225 K	
	Qm	Cl	Qm	Cl	Qm	Cl
ω_1	18	56	30	25	8	15
ω_2	38	22	37	19	30	41
ω_3	8	7	13	7	0	0
ω_4	3	5	0	0	0	0
ω_5	10	4	0	11	0	0
ω_6	11	4	4	3	0	4

stagger opp are less than 10 %. Moreover, the ratio of the first lowest vibrational mode (torsion oop) is also found to increase from temperature of 75 to 150 K and then decrease at 225 K, whereas that of second lowest one (butterfly oop) decrease with increasing temperature.

We finally discuss the cross-shaped distribution in Fig. 5c. As indicated in Table 3, the ratios of ω_1 (torsion oop) and ω_3 (opening ip) increase with increasing temperature. Meanwhile, the ratios of ω_2 (butterfly oop) and ω_6 (stretching ip) decrease with increasing temperature. The ω_1 and ω_2 are the motion that $R_{N1\cdots N2}$ and $R_{N3\cdots N4}$ maintain, and ω_3 is the motion that $R_{N1\cdots N2}$ and $R_{N3\cdots N4}$ enlarge alternately, while ω_6 is the motion that $R_{N1\cdots N2}$ and $R_{N3\cdots N4}$ enlarge simultaneously. Therefore, the cross-shaped distribution in Fig. 5c is from the increasing ω_3 and decreasing ω_6 due to thermal fluctuation.

4 Conclusions

Classical molecular dynamics (MD) and path integral molecular dynamics (PIMD) simulations have been carried out for hydrogen-bonded structure of $7AI_2$ normal form in the gas phase at 75, 150, and 225 K using PM6 method. The average NH bond distances are found to be longer in the quantum simulations where both thermal and quantum fluctuations to anharmonic vibration are taken into account. We found the large difference for the relationship with respect to two distances of two heavy atoms N···N between 75 and 150 K in quantum simulation. This is because the N···N distance is correlated with H···N distance, but not with NH distance. At 150 K, the quantum effect is found to enhance the H-bonding. These shorter values of hydrogen-bonded distances are obvious at 225 K because the 7AI monomer starts to dissociate from each other in the $7AI_2$, and the dissociation of $7AI_2$ was observed at 300 K both in quantum and classical simulations.

In addition, the principal component analysis was applied to analyze the contribution of low vibrational modes. The ratio of dimer butterfly out-of-plane mode, which is the second lowest vibrational motion from normal mode analysis and the most dominant motion, decreases with increasing temperature, while that of the first lowest vibration mode (dimer torsion out-of-plane) increases from temperature 75 to 150 K and then decreases at 225 K both in quantum and classical simulations. Furthermore, the motions of two hydrogen-bonded structures are significantly different with increasing temperature. This is because the ratios of opening in-plane and stretching in-plane motions decrease.

Acknowledgments The present study has been supported by Grant-in-aid for Scientific Research by Ministry of Education, Culture, Spots, Science and Technology, Japan. N. Kungwan wishes to thank the Thailand Research Fund (TRG5680098) for financial support. Department of Chemistry, Faculty of Science, Chiang Mai University, Chiang Mai, Thailand is also acknowledged.

References

1. Jeffrey GA, Saenger W (1991) Hydrogen bonding in biological structures. Springer, New York
2. Goodman MF (1995) DNA models: mutations caught in the act. Nature 378(6554):237–238
3. Al-Taylor C, Ashraf el-Bayoumi M, Kasha M (1969) Excited-state two-proton tautomerism in hydrogen-bonded n-heterocyclic base pairs. Proc Natl Acad Sci 63(2):253–260
4. Catalan J, Kasha M (2000) Photophysics of 7-azaindole, tts doubly-H-bonded base-pair, and corresponding proton-transfer-tautomer dimeric species, via defining experimental and theoretical results. J Phys Chem A 104(46):10812–10820
5. Douhal A, Kim SK, Zewail AH (1995) Femtosecond molecular-dynamics of tautomerization in model base-pairs. Nature 378(6554):260–263
6. Sekiya H, Sakota K (2008) Excited-state double-proton transfer in a model DNA base pair: resolution for stepwise and concerted mechanism controversy in the 7-azaindole dimer revealed by frequency- and time-resolved spectroscopy. J Photochem Photobiol C Photochem Rev 9(2):81–91
7. Kwon OH, Zewail AH (2007) Double proton transfer dynamics of model DNA base pairs in the condensed phase. Proc Natl Acad Sci USA 104(21):8703–8708
8. Takeuchi S, Tahara T (2001) Excitation-wavelength dependence of the femtosecond fluorescence dynamics of 7-azaindole dimer: further evidence for the concerted double proton transfer in solution. Chem Phys Lett 347(1–3):108–114
9. Takeuchi S, Tahara T (2007) The answer to concerted versus step-wise controversy for the double proton transfer mechanism of 7-azaindole dimer in solution. Proc Natl Acad Sci USA 104(13):5285–5290

10. Suzuki T, Okuyama U, Ichimura T (1997) Double proton transfer reaction of 7-azaindole dimer and complexes studied by time-resolved thermal lensing technique. J Phys Chem A 101(38):7047–7052
11. Tokumura K, Watanabe Y, Itoh M (1984) A transient absorption and two-step laser excitation fluorescence study of the double proton transfer of 7-azaindole H-bonded dimers in 3-methylpentane. Chem Phys Lett 111(45):379–382
12. Tokumura K, Watanabe Y, Itoh M (1986) Deuterium isotope effects of excited-state and ground-state double-proton-transfer processes of the 7-azaindole H-bonded dimer in 3-methylpentane. J Phys Chem 90(11):2362–2366
13. Tokumura K, Watanabe Y, Udagawa M, Itoh M (1987) Photochemistry of transient tautomer of 7-azaindole hydrogen-bonded dimer studied by two-step laser excitation fluorescence measurements. J Am Chem Soc 109(5):1346–1350
14. Yokoyama H, Watanabe H, Omi T, Ishiuchi S-I, Fujii M (2001) Structure of hydrogen-bonded clusters of 7-azaindole studied by IR dip spectroscopy and ab initio molecular orbital calculation. J Phys Chem A 105(41):9366–9374
15. Hazra MK, Mukherjee M, Ramanathan V, Chakraborty T (2012) Structure and intermolecular vibrations of 7-azaindole-water 2:1 complex in a supersonic jet expansion: laser-induced fluorescence spectroscopy and quantum chemistry calculation. J Chem Sci 124(1):131–139
16. Catalan J, Perez P, del Valle JC, de Paz JLG, Kasha M (2002) The concerted mechanism of photo-induced biprotonic transfer in 7-azaindole dimers: a model for the secondary evolution of the classic C2h dimer and comparison of four mechanisms. Proc Natl Acad Sci 99(9):5799–5803
17. Dreyer J (2007) Unraveling the structure of hydrogen bond stretching mode infrared absorption bands: an anharmonic density functional theory study on 7-azaindole dimers. J Chem Phys 127(5):054309
18. Dwyer JR, Dreyer J, Nibbering ETJ, Elsaesser T (2006) Ultrafast dynamics of vibrational N–H stretching excitations in the 7-azaindole dimer. Chem Phys Lett 432(13):146–151
19. Ishikawa H, Yabuguchi H, Yamada Y, Fujihara A, Fuke K (2010) Infrared spectroscopy of jet-cooled tautomeric dimer of 7-azaindole: a model system for the ground-state double proton transfer reaction. J Phys Chem A 114(9):3199–3206
20. Ishikawa H, Nakano T, Takashima T, Yabuguchi H, Fuke K (2013) Deuteration effect on the NH/ND stretch band of the jet-cooled 7-azaindole and its tautomeric dimers: relation between the vibrational relaxation and the ground-state double proton-transfer reaction. Chem Phys 419:101–106
21. Brauer B, Gerber RB, Kabelac M, Hobza P, Bakker JM, Abo Riziq AG, de Vries MS (2005) Vibrational spectroscopy of the G-C base pair:‰ experiment, harmonic and anharmonic calculations, and the nature of the anharmonic couplings. J Phys Chem A 109(31):6974–6984
22. Ishibashi H, Hayashi A, Shiga M, Tachikawa M (2008) Geometric isotope effect on the N2H7+ cation and N2H5− anion by ab initio path integral molecular dynamics simulation. ChemPhysChem 9(3):383–387
23. Yagi K, Karasawa H, Hirata S, Hirao K (2009) First-principles quantum calculations on the infrared spectrum and vibrational dynamics of the guanine–cytosine base pair. ChemPhysChem 10(9–10):1442–1444
24. Pérez A, Tuckerman ME, Hjalmarson HP, von Lilienfeld OA (2010) Enol tautomers of Watson–Crick base pair models are metastable because of nuclear quantum effects. J Am Chem Soc 132(33):11510–11515. doi:10.1021/ja102004b
25. Daido M, Kawashima Y, Tachikawa M (2013) Nuclear quantum effect and temperature dependency on the hydrogen-bonded structure of base pairs. J Comput Chem 34(28):2403–2411
26. Daido M, Koizumi A, Shiga M, Tachikawa M (2011) Nuclear quantum effect on the hydrogen-bonded structure of guanine–cytosine pair. Theor Chem Acc 130(2–3):385–391
27. Stewart JJP (2007) Optimization of parameters for semiempirical methods V: modification of NDDO approximations and application to 70 elements. J Mol Model 13(12):1173–1213
28. MOPAC2009 (2008) James J. P. Stewart, Stewart computational chemistry. Colorado Spring, CO, USA. http://OpenMOPAC.net
29. Ahlrichs R, Baer M, Haeser M, Horn H, Koelmel C (1989) Electronic structure calculations on workstation computers: the program system turbomole. Chem Phys Lett 162(3):165–169
30. Frisch MJ, Trucks GW, Schelegel HB et al (2003) GAUSSIAN 03, Revision B. 05. Gaussian Inc., Pittsburgh, PA
31. Martyna GJ, Klein ML, Tuckerman M (1992) Nosé–Hoover chains: the canonical ensemble via continuous dynamics. J Chem Phys 97(4):2635–2643
32. Kawashima Y, Tachikawa M (2014) Ab initio path integral molecular dynamics study of the nuclear quantum effect on out-of-plane ring deformation of hydrogen maleate anion. J Chem Theory Comput 10(1):153–163
33. Marx D, Parrinello M (1994) Ab initio path-integral molecular dynamics. Z Phys B Condens Matter 95 (Copyright (C) 2014 American Chemical Society (ACS). All Rights Reserved.):143–144
34. Marx D, Parrinello M (1996) Ab initio path integral molecular dynamics: basic ideas. J Chem Phys 104(11):4077–4082
35. Cao J, Martyna GJ (1996) Adiabatic path integral molecular dynamics methods. II. Algorithms. J Chem Phys 104(5):2028–2035
36. Suzuki K, Tachikawa M, Shiga M (2010) Efficient ab initio path integral hybrid Monte Carlo based on the fourth-order Trotter expansion: application to fluoride ion-water cluster. J Chem Phys 132(14):144108
37. Cao J, Berne BJ (1993) A Born–Oppenheimer approximation for path integrals with an application to electron solvation in polarizable fluids. J Chem Phys 99(4):2902–2916
38. Tuckerman ME, Marx D, Klein ML, Parrinello M (1996) Efficient and general algorithms for path integral Car–Parrinello molecular dynamics. J Chem Phys 104(14):5579–5588
39. Shiga M, Tachikawa M, Miura S (2001) A unified scheme for ab initio molecular orbital theory and path integral molecular dynamics. J Chem Phys 115(20):9149–9159
40. Kawashima Y, Tachikawa M (2013) Nuclear quantum effect on intramolecular hydrogen bond of hydrogen maleate anion: an ab initio path integral molecular dynamics study. Chem Phys Lett 571:23–27
41. Yu XF, Yamazaki S, Taketsugu T (2011) Concerted or stepwise mechanism? CASPT2 and LC-TDDFT study of the excited-state double proton transfer in the 7-azaindole dimer. J Chem Theory Comput 7(4):1006–1015
42. Tachikawa M, Shiga M (2005) Geometrical H/D isotope effect on hydrogen bonds in charged water clusters. J Am Chem Soc 127(34):11908–11909
43. Suzuki K, Shiga M, Tachikawa M (2008) Temperature and isotope effects on water cluster ions with path integral molecular dynamics based on the fourth order Trotter expansion. J Chem Phys 129(14):144310
44. Koizumi A, Suzuki K, Shiga M, Tachikawa M (2011) Communication: a concerted mechanism between proton transfer of Zundel anion and displacement of counter cation. J Chem Phys 134(3):031101
45. Folmer DE, Poth L, Wisniewski ES, Castleman AW Jr (1998) Arresting intermediate states in a chemical reaction on a femtosecond time scale: proton transfer in model base pairs. Chem Phys Lett 287(12):1–7
46. Folmer DE, Wisniewski ES, Hurley SM, Castleman AW (1999) Femtosecond cluster studies of the solvated 7-azaindole

excited state double-proton transfer. Proc Natl Acad Sci USA 96(23):12980–12986
47. Kitao A, Hirata F, Gō N (1991) The effects of solvent on the conformation and the collective motions of protein: normal mode analysis and molecular dynamics simulations of melittin in water and in vacuum. Chem Phys 158(2–3):447–472
48. Kawashima Y, Sugita Y, Yoda T, Okamoto Y (2005) Effects of the fixed end in single-molecule imaging techniques: a replica-exchange molecular dynamics simulation study. Chem Phys Lett 414(4–6):449–455
49. Kitao A, Go N (1999) Investigating protein dynamics in collective coordinate space. Curr Opin Struct Biol 9(2):164–169
50. Potoyan DA, Papoian GA (2011) Energy landscape analyses of disordered histone tails reveal special organization of their conformational dynamics. J Am Chem Soc 133(19):7405–7415
51. Yang L-W, Eyal E, Bahar I, Kitao A (2009) Principal component analysis of native ensembles of biomolecular structures (PCA_NEST): insights into functional dynamics. Bioinformatics 25(5):606–614